Surface plasmon-based nanopatterning assisted by gold nanospheres

2008 Nanotechnology 19 025305

(http://iopscience.iop.org/0957-4484/19/2/025305)

Nanotechnology **19** (2008) 025305 (6pp) doi:10.1088/0957-4484/19/02/025305

Surface plasmon-based nanopatterning assisted by gold nanospheres

Alex Heltzel, Senthil Theppakuttai, S C Chen and John R Howell

The University of Texas at Austin, Austin, TX 78712, USA

Received 21 September 2007, in final form 23 October 2007
Published 6 December 2007
Online at stacks.iop.org/Nano/19/025305

Abstract

A pulsed laser is used to produce surface plasmon excitation in a monolayer of gold (Au) spheres to nanopattern a silicon substrate. An electrodynamic model accompanies the experimental data, based on the numerical solution to the complete Maxwell's equations including near- and far-field effects and reflection from the substrate. The Drude-employing finite-difference time-domain method describes the deformation and enhancement of the laser pulse around the boundary of a Au sphere and the resulting distribution of intensity incident upon the substrate. The effect of the incident laser angle on the plasmon generation and lithographic potential is studied.

Nomenclature

E	electric field vector
H	magnetic field vector
J	electric current density
β	Drude dispersion coefficient
ε	electrical permittivity
ε_∞	relative permittivity at infinite frequency
γ_P	inverse of Drude pole relaxation time
k_D	Drude dispersion coefficient
μ	magnetic permeability
ω_P	frequency of Drude pole

1. Introduction

The miniaturization of conventional photonic devices is limited by diffraction effects due to the wave nature of light. In order to push the miniaturization of optical elements and devices, new concepts are needed. In this context, research has recently intensified on noble metal nanoparticles (Klar *et al* 1998). Within such particles visible light can resonantly excite collective electron oscillations, also known as surface plasmons (Raether 1988). Surface plasmon resonances in metallic nanoparticles are of interest for a variety of applications due to the large enhancement and localization of the electromagnetic field at the metal/dielectric boundary. Recent advances that allow metals to be structured and characterized on the nanometer scale have facilitated this research.

Surface plasmons can be categorized into two types: localized plasmon resonances (Hutter and Fendler 2004), in which incident light is absorbed or scattered by the oscillating electric dipoles within a metal nanoparticle; and surface plasmon polaritons (Sambles *et al* 1991), which propagate along metal surfaces in a waveguide-like fashion until released at some distance from their point of origin. The former are important for generating local field factors, which enhance linear and nonlinear optical effects near the metal surface. However, metal nanostructures often support both types of plasmons simultaneously. It is the particle plasmon effect that is utilized in this study for the nanoscale modification of solids. Nevertheless, the plasmonic coupling of metal nanoparticles with light enhances a broad range of useful optical phenomena, such as resonant light scattering, surface plasmon resonance (Murray *et al* 2004), and surface-enhanced Raman scattering (Grand *et al* 2005), all of which have tremendous potential for ultrasensitive chemical and biomolecular detection and analysis.

Recently, a new field named 'plasmonic nanolithography' has emerged. Blaikie and McNab (2001) outlined the basis of evanescent interferometric lithography (EIL) by calculating field intensity near illuminated chrome diffraction gratings. The results suggested the ability to pattern substrates with localized enhancements well below the diffraction limit. Paulus *et al* (2001) performed calculations using the Green's tensor technique which quantified the near-field effects of chrome and gold masks, and the presence of surrounding dielectric material. Luoa and Ishihara (2004) patterned sub-100 nm lines photolithographically using surface plasmon polariton interference in the optical near-field excited by a wavelength of 436 nm. Using 2D hole arrays on an aluminum substrate, features as small as 90 nm have been realized (Srituravanich *et al* 2004). Instead of using metallic masks

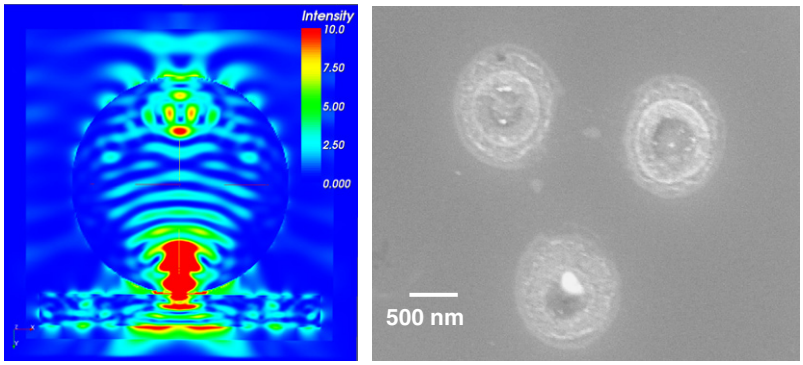

Figure 1. Predicted field enhancement (FDTD) due to scattering of laser energy by 1.76 μm dielectric microsphere, and experimentally observed surface modification (SEM).

to generate the plasmon resonance, silver nanospheres have been used and features as small as 50 nm were obtained (Kik *et al* 2002). However, since all the above mentioned works were developed as a parallel route to optical lithography, they focused only on patterning photoresists.

In this work, plasmons are used to directly pattern various substrates. This is achieved by illuminating gold nanospheres at their resonant frequency by using a 532 nm laser beam. The field enhancement as a result of this excitation is directly absorbed by the substrate and nanofeatures are realized. The features thus obtained are characterized using a scanning electron microscope. The effect of the substrate, sphere size, laser energy, polarization, and incidence angle has been studied both theoretically and experimentally.

Previous work (Heltzel *et al* 2007) has utilized the evanescent near-field surrounding dielectric microspheres to perform nanoscale optical lithography. The mechanism of energy enhancement in the case of dielectric microstructures is the scattering of the incident radiation and optical field convergence near the substrate surface. This effect has been used by both short-pulse and ultrafast fs lasers with incidence normal to the substrate to generate various lithographic results. The theoretical and experimental characterizations of these dielectric experiments are shown in figure 1. Contrary to these experiments, the lithographic technique presented here is based on the physical behavior of surface plasmon polaritons. It will be shown that the interaction of laser energy and metallic micro/nanospheres differs significantly from that of dielectric spheres, requiring adjusted operating procedure, and resulting in a different lithographic potential.

2. Plasmonic modeling

To predict potential lithographic results due to plasmon excitation of gold spheres, a 3D computational electrodynamics program was built based on the finite-difference time-domain (FDTD) method. The current density forms of Maxwell's equations are used, in order to treat negative real parts of the dielectric function defining a metallic response as well as positive values defining dielectrics.

$$\frac{\partial E}{\partial t} = \frac{1}{\varepsilon}[\nabla \times H - J] \tag{1a}$$

$$\frac{\partial H}{\partial t} = -\frac{1}{\mu}[\nabla \times E] \tag{1b}$$

$$\frac{\partial J}{\partial t} = k_d J + \beta E \tag{1c}$$

where J is the electric current density vector, and k_d and β are material-based coefficients. The frequency-dependent optical properties of the nanospheres are approximated by the Drude model, which defines the dispersive permittivity as

$$\varepsilon(\omega) = \varepsilon_\infty - \frac{\omega_P^2}{\omega^2 + j\omega\gamma_P} \tag{2}$$

in which case the coefficients of equation (1) are $\varepsilon = \varepsilon_\infty * \varepsilon_0$, $k_d = -\gamma_P$, and $\beta = \varepsilon_0$. The constants $\varepsilon_\infty = 9.5$, $\gamma_P = 0.069\,09$ eV, and $\omega_P = 8.9488$ eV for gold are obtained from the work of Johnson and Christy (1972).

The details of the FDTD algorithm are covered in depth elsewhere (Taflove and Hagness 2005) and therefore will not be addressed in this paper. The code was verified successfully against the analytical solution for a radiating dipole. The convolutional perfectly matched layer (CPML) (Gedney 1996) was employed as an absorbing boundary condition, and the total field/scattered field construct (Yee 1966) was used to generate the plane wave of the incident laser. Matched numerical dispersion was included to eliminate diffusive numerical error in long duration (time step) runs.

Four scenarios were modeled and are presented here. Solitary 250 nm gold spheres resting on a silicon substrate were irradiated with a $\lambda = 532$ nm Nd:YAG laser at incident angles $\theta = 0°$ (parallel to substrate), 45°, and 90° (normal to substrate). A single 40 nm gold sphere is also modeled with laser incidence parallel to the substrate. The laser is polarized perpendicular to the propagation direction in both simulation and experiment. Plasmon generation is expected in the polarization direction.

Figures 2(a) and (b) show the electromagnetic intensity cross-sections due to a 0° incident laser angle (parallel to substrate). The plasmonic enhancement is evident at the bottom of the nanosphere, corresponding to the polarization axis. Figure 2(b) shows the energy profile the silicon would 'see'. It is clear that a very localized area of significantly enhanced energy is present, which can be utilized

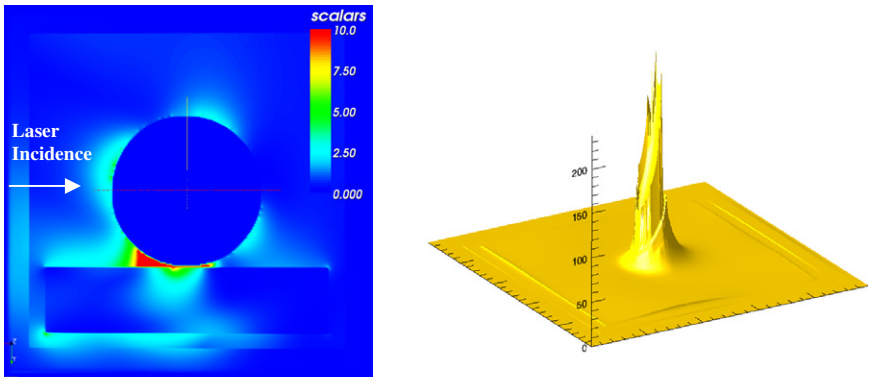

(a) (b)

Figure 2. FDTD plasmon simulation around a 250 nm Au sphere, 0° incident angle; (a) vertical slice of 3D intensity distribution, (b) distribution on surface of silicon substrate, 625 nm × 625 nm.

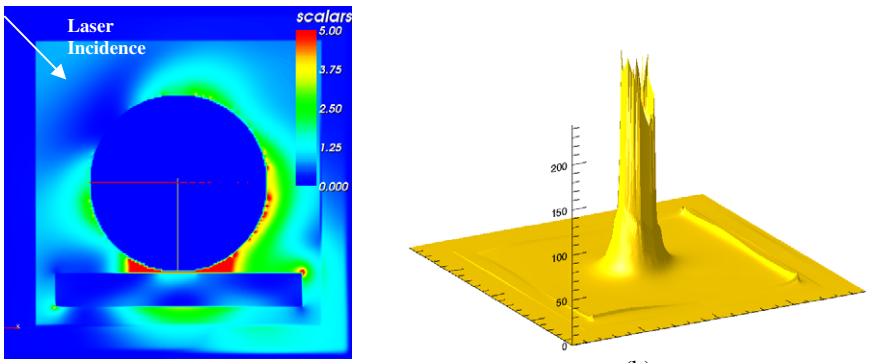

(a) (b)

Figure 3. FDTD plasmon simulation around a 250 nm Au sphere, 45° incident angle; (a) vertical slice of 3D intensity distribution, (b) distribution on surface of silicon substrate, 625 nm × 625 nm.

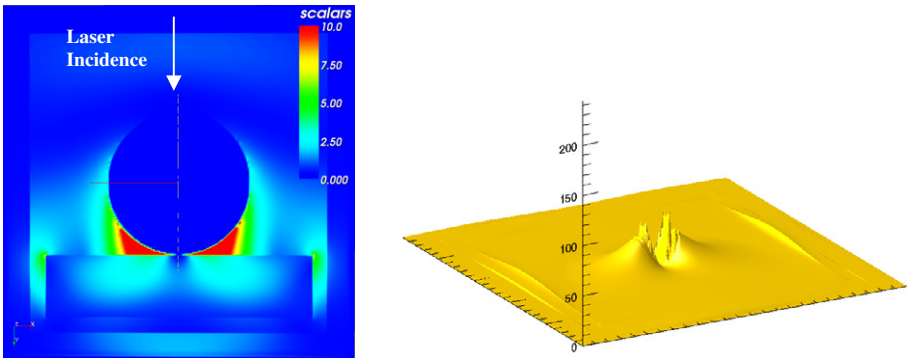

(a) (b)

Figure 4. FDTD plasmon simulation around a 250 nm Au sphere, 90° incident angle; (a) vertical slice of 3D intensity distribution, (b) distribution on surface of silicon substrate, 625 nm × 625 nm.

for nanopatterning purposes. A moderate enhancement is present within a 100 nm spot size, and an increased intensity spike is present at a scale of 10–20 nm. The scale of figures 2(b), 3(b), and 4(b) are 625 nm × 625 nm.

Figures 3(a) and (b) give the laser/sphere interaction for a more practical case of a 45° incident angle. This angle could be expected to irradiate large arrays of spheres while maintaining a significant component of polarization directed toward the substrate. The figures indicate a strong plasmonic enhancement and a coupling of the energy between the silicon and gold interfaces. Again, the enhanced intensity is confined within a 100 nm spot size.

Figures 4(a) and (b) show the profiles from the 90° normal incident angle. Whereas the plasmons surrounding a sphere

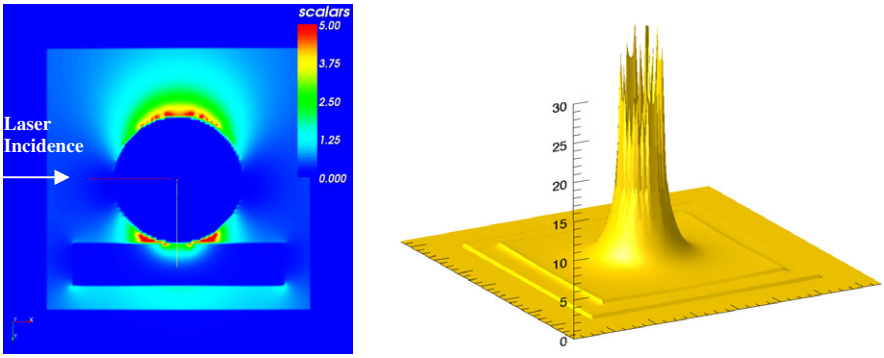

Figure 5. FDTD plasmon simulation around a 40 nm Au sphere, 0° incident angle; (a) vertical slice of 3D intensity distribution, (b) distribution on surface of silicon substrate, 100 nm × 100 nm.

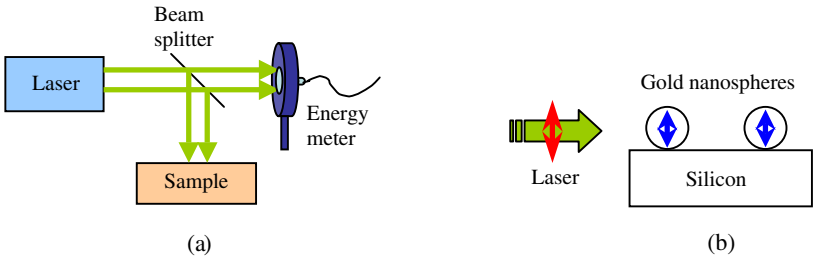

Figure 6. Schematic of (a) the experimental set-up, and (b) illumination of gold spheres with the laser beam.

in vacuum would be solely along the polarization direction, the silicon serves to draw them toward the contact area. The overall enhancement is severely diminished, however, compared to the 0° and 45° cases, which would limit the lithographic capability. These results contrast with the same experiment using a dielectric sphere shown in figure 1, which exhibit a solitary peak of enhancement (generally lower in magnitude) directed along the axis of laser propagation.

Finally, figures 5(a) and (b) show the predicted enhancement surrounding a 40 nm gold sphere irradiated at an angle 0°, parallel to the substrate. The overall enhancement is weaker than surrounding the larger spheres, but can still be utilized for lithographic purposes as will be shown. The scale of figure 5(b) is now 100 nm × 100 nm. The dimensional lower limit of the FDTD capability is approached when modeling such small structures. In order to resolve the shape of the sphere, node spacing in the numerical scheme must be on the order of ångströms. The time steps used must be smaller than the time for light to propagate across nodes. Three dimensional environments containing several hundred million nodes such as these presented can therefore require the speed and memory only available in massively parallel systems. On an individual workstation with dual 3.0 GHz processors and 4 GB RAM, a single simulation requires up to 72 h.

3. Experimental set-up

The schematic of our experimental set-up is shown in figure 6(a). A pulsed Nd:YAG laser of wavelength 532 nm and pulse width 10 ns is used for the experiment. The output from the laser is passed through a half wave plate, which by rotating changes the polarization of the laser beam from horizontal to vertical and vice versa. The laser beam is then split into two by using a beam splitter—one part to be used for patterning and the other for measuring the laser energy. The sample is mounted on a 3D stage and the laser beam is focused onto the sample by using a plano-convex lens.

As shown in figure 6(b), gold spheres are irradiated with a p-polarized laser beam at a glancing angle, i.e. parallel to the substrate. Since the diameter of the gold sphere is much smaller than the illuminating laser wavelength, this results in an oscillating dipole around the particle resulting in a strongly enhanced electrical field near the sphere as described in the theoretical analysis. This resonantly excited field is absorbed by the substrate leading to formation of nanofeatures. The features thus obtained were characterized using a scanning electron microscope.

The first sample used for patterning is a 500 μm thick n-type (100) polished silicon wafer with a surface roughness of a few nanometers (<2 nm) and a 2–3 nm thick native oxide layer. Before processing the sample, care was taken to ensure that the sample is clean and free of any contaminants. For this reason, it is first cleaned in ethanol solution followed by rinsing in deionized water. After the sample is dried with nitrogen gas, a colloidal suspension of mono-dispersed gold spheres is applied on the silicon sample and let to dry. The gold solution is diluted in order to scatter the gold spheres deposited on the surface. A scanning electron microscope image of the scattered 40 nm gold spheres on silicon is presented in figure 7.

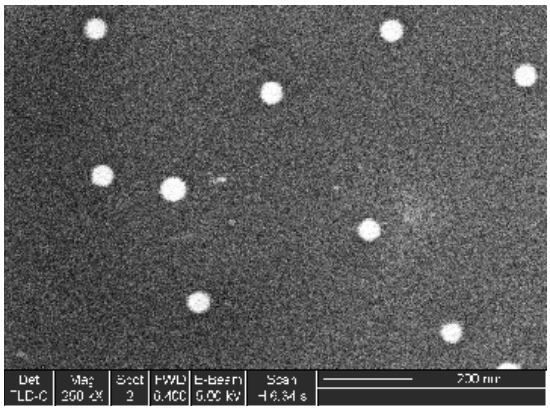

Figure 7. Scanning electron micrograph of the 40 nm gold spheres deposited on silicon.

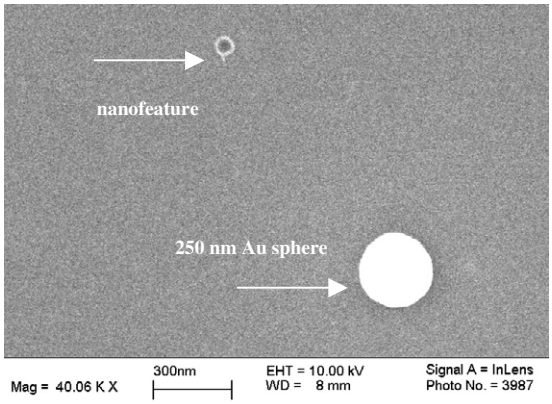

Figure 8. SEM micrograph of the features on silicon obtained by irradiating 250 nm gold spheres with a 532 nm laser at 50 mJ cm^{-2} fluence.

4. Experimental results

The experiment is performed on three different materials (silicon, polyimide, and PMMA) using gold spheres of different diameters (250 and 40 nm). The effect of laser polarization (s and p polarization) at various incident angles (0° and 90°) is studied in detail in order to understand the role of each of these parameters. In the case of 250 nm gold spheres, approximately 100 nm features are created. An SEM image of the features formed at a laser fluence of 50 mJ cm^{-2} is shown in figure 8. For the case of 40 nm gold spheres irradiated at a fluence of 50 mJ cm^{-2}, the features obtained are roughly the diameter of the sphere or slightly smaller. Figure 9 demonstrates optical lithography with a full order of magnitude below the diffraction limit. The feature sizes correlates well with the FDTD-predicted enhanced intensity distributions given in figures 2 and 5.

Features very similar to those shown in figures 8 and 9 were also observed with the use of polyimide substrates. In order to make sure the formation of nanofeatures is purely due to the optical excitation of plasmons and not the heating of gold spheres, polymethylmethacrylate (PMMA) is used as an additional substrate. PMMA is chosen because of its

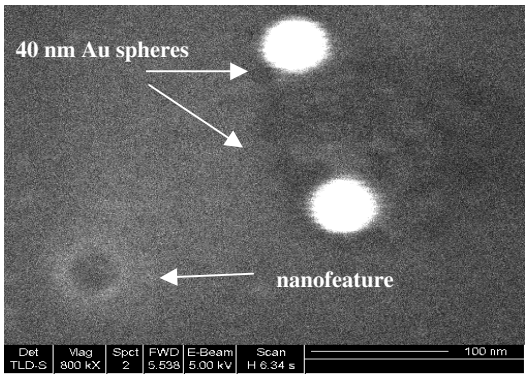

Figure 9. SEM micrograph of features on silicon obtained by irradiating 40 nm gold spheres with 532 nm laser at 50 mJ cm^{-2} fluence.

poor absorption characteristic at this wavelength. First, a silicon sample is cleaned in ethanol and using a spin coater at 1200 rpm for 90 s PMMA is spin-coated on the silicon substrate. This is followed by baking the sample in an oven at 120 F for 1 h to improve the adhesion. As before, gold spheres are deposited by applying a drop of the gold solution and letting it to dry. When the spheres are irradiated with the 532 nm laser beam, no such nanofeatures were observed. This confirms that the features formed on silicon and polyimide is not because of the heating of gold, but rather due to the electric field enhancement around the nanospheres.

The mechanism of nanostructuring the silicon and polyimide materials is likely a combination of surface vaporization and redistribution of molten material. The nanosecond timescale of energy deposition to the substrates is sufficient to permit thermodynamic equilibrium in the electron and lattice systems, thereby precluding ablation as a dominant material removal mechanism. Laser-induced vaporization and liquid expulsion due to nanosecond irradiation has been described theoretically by Chan and Mazumder (1987) and later by Ho *et al* (1995). They performed calculations on the assumption that temperatures in the penetration depth of the melted regime are sufficient to initiate surface liquid/vapor phase transition. In addition, previous work (Lu *et al* 2003) has shown that surface tension forces beneath irradiated microspheres are responsible for redistributing molten material into bowl and sombrero shapes. No detailed fluid dynamic calculations are presented in the current work, however.

The effect of two angles of incidence—normal incidence (90°) and glancing incidence (0°), were studied. Nanofeatures were observed only for the p-polarized glancing incidence and not for the normal incidence (irrespective of the polarization). This is understood from the FDTD results presented in figures 2–5, where only under glancing incidence and p polarization is the plasmon oscillation directed at the substrate.

5. Conclusions

Features as small as 40 nm ($\lambda/15$) have been realized on various substrates by overcoming the diffraction limit of light. This is achieved by irradiating gold nanospheres

using a 532 nm Nd:YAG laser and inducing collective plasma oscillations inside the nanoparticle. The electrical field enhancement resulting from this oscillation is absorbed by the substrate and nanofeatures are created. The finite-difference time-domain method has been employed to model plasmonic enhancement, and the predictions correlate well with experimental characterizations. With this verification, computational modeling can be considered a predictive tool to assist in the development of nano-optical lithography and plasmonic propagation technologies.

Acknowledgments

The authors wish to acknowledge support from the National Science Foundation under Grant CTS-0243160 and from the University of Texas Advanced Manufacturing Center.

References

Blaikie R J and McNab S J 2001 Evanescent interferometric lithography *Appl. Opt.* **40** 1692–7

Chan C L and Mazumder J 1987 One-dimensional steady-state model for damage by vaporization and liquid expulsion due to laser–material interaction *J. Appl. Phys.* **62** 4579–86

Gedney S D 1996 An anisotropic PML absorbing media for FDTD simulation of fields in lossy dispersive media *Electromagnetics* **16** 399–415

Grand J, de la Chapelle M L, Bijeon J-L, Adam P-M, Vial A and Royer P 2005 Role of localized surface plasmons in surface-enhanced Raman scattering of shape-controlled metallic particles in regular arrays *Phys. Rev.* B **72** 33407

Heltzel A, Battula A, Chen S C and Howell J R 2007 Nanostructuring borosilicate glass with near-field enhanced energy using a femtosecond laser pulse *J. Heat Transfer* **129** 53–9

Ho J R, Grigoropoulos C P and Humphrey J A C 1995 Computational study of heat transfer and gas dynamics in the pulsed laser evaporation of metals *J. Appl. Phys.* **78** 4696–709

Hutter E and Fendler H 2004 Exploitation of localized surface plasmon resonance *Adv. Mater.* **16** 1685–706

Johnson P B and Christy R W 1972 Optical constants of noble metals *Phys. Rev.* B **6** 4370–9

Kik P G, Maier S A and Atwater H A 2002 Plasmon printing—a new approach to near-field lithography *Nanopatterning—From Ultralarge-Scale Integration to Biotechnology. Symposium (Materials Research Society Symposium Proceedings)*

Klar T A, Perner M, Grosse S, Plessen G, Spirkl W and Feldmann J 1998 Surface-plasmon resonances in single metallic particles *Phys. Rev. Lett.* **80** 4249–52

Lu Y, Theppakuttai S and Chen S C 2003 Marangoni effect in nanosphere-enhanced laser nanopatterning of silicon *Appl. Phys. Lett.* **82** 4143–5

Luoa X and Ishihara T 2004 Surface plasmon resonant interference nanolithography technique *Appl. Phys. Lett.* **84** 4780–2

Murray W A, Astilean S and Barnes W L 2004 Transition from localized surface plasmon resonance to extended surface plasmon–polariton as metallic nanoparticles merge to form a periodic hole array *Phys. Rev.* B **69** 165407

Paulus M, Schmid H, Michel B and Martin O J F 2001 Contrast mechanisms in high-resolution contact lithography: a comparative study *Microelectron. Eng.* **57/58** 109–16

Raether H 1988 *Surface Plasmons* (Berlin: Springer)

Sambles J R, Bradbery G W and Yang F 1991 Optical excitation of surface plasmons: an introduction *Contemp. Phys.* **32** 173–83

Srituravanich W, Fang N, Sun C, Luo Q and Zhang X 2004 Plasmonic nanolithography *Nano Lett.* **4** 1085–8

Taflove A and Hagness S 2005 *Computational Electrodynamics* 3rd edn (Boston, MA: Artech House)

Yee K S 1966 Numerical solution of initial boundary value problems involving Maxwell's equations in isotropic media *IEEE Trans. Antennas Propag.* **14** 302–7